

RESEARCH ARTICLE

# Tracking mesoscale convective systems in central equatorial Africa

Adam T. Hartman 

NOAA Climate Prediction Center, College Park, Maryland

## Correspondence

Adam T. Hartman, NOAA Climate Prediction Center, 5830 University Research Ct, College Park, MD 20740.  
Email: adam.hartman@noaa.gov

## Funding information

Division of Atmospheric and Geospace Sciences, Grant/Award Number: NSF AGS 1535439

## Abstract

The Congo basin in central equatorial Africa is home to some of the most intense convection in the global tropics. Mesoscale convective systems (MCSs) provide much of the annual rainfall over this region during the March–April–May (MAM) and September–October–November (SON) rainy seasons. Features of these systems are essential to rainfall variability in this region and greatly impact human health, agriculture, livestock, and drought monitoring. Knowledge of variability is hindered by the lack of in-situ observations and meteorological stations. The present study identifies and tracks MCSs for the 33-year period 1983–2015 for MAM and SON. MCS and environmental parameters are calculated for the rainy seasons using satellite and reanalysis data. Spatial distributions of MCS parameters and diurnal cycles for select MCS parameters are compared to prior research. Statistical significance testing is performed to determine if there are meaningful differences between the seasons. Seasonal differences are briefly discussed. 650 hPa relative vorticity patterns suggest localized terrain effects may play a role near a local maximum in MCS initiation frequency in the lee of the Great Rift Valley. Spatial distributions of 33-year MCS counts, trajectories, speeds, sizes, maximum intensities, and durations, based on initiation locations, agree well with prior research. Differences between seasons are statistically significant and variable and latitude dependent. There is high interannual variability among all MCS and environmental parameters.

## KEYWORDS

Congo, mesoscale, convection, Africa, climatology, MCS, rainfall, variability, propagation

## 1 | INTRODUCTION

Rainfall variability in the Congo basin has important economic implications related to human health, agriculture, livestock, and drought monitoring (Sandjon *et al.*, 2012). Rainfall is shown to be a major climatic control on

rainforest dynamics and the hydrologic cycle in the Congo basin, but knowledge of variability is hindered by the lack of in-situ observations and meteorological stations (Hua *et al.*, 2019). Several satellite precipitation products provide rainfall estimates over this region. However, their reliability is region and product dependent

This is an open access article under the terms of the Creative Commons Attribution License, which permits use, distribution and reproduction in any medium, provided the original work is properly cited.

© 2020 The Author. International Journal of Climatology published by John Wiley & Sons Ltd on behalf of the Royal Meteorological Society.

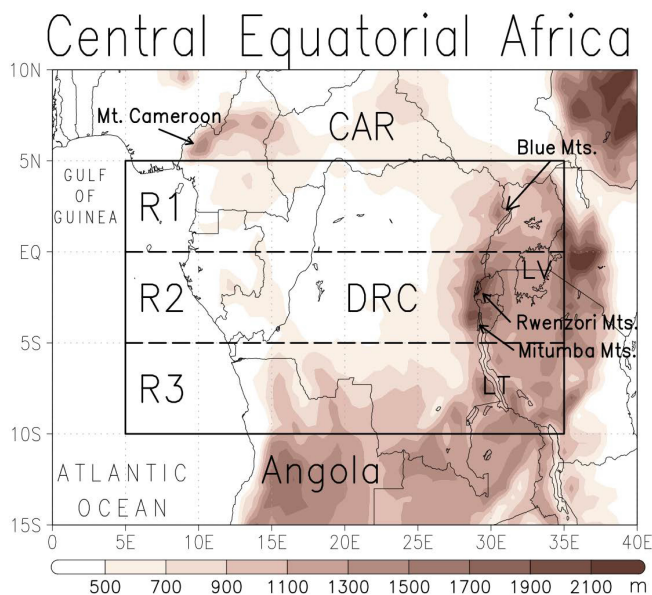


**FIGURE 1** Regions (dashed black lines) within central equatorial Africa (solid black box) and topography (shading). Acronyms are represented as follows: R1, region 1; R2, region 2; R3, region 3; CAR, Central African Republic; DRC, Democratic Republic of the Congo; LV, Lake Victoria; LT, Lake Tanganyika [Colour figure can be viewed at [wileyonlinelibrary.com](http://wileyonlinelibrary.com)]

and inherent errors may be introduced via ground truth dependencies, measurement biases, and poor temporal resolution (Camberlin *et al.*, 2019).

The present study is focused in central equatorial Africa (CEA), a region covering 5°N–10°S latitude and 5°–35°E longitude, centered over the Congo basin (Figure 1). The Congo rainforest receives on the order of 2000 mm of rainfall annually (Liebmann *et al.*, 2012; Washington *et al.*, 2013). Roughly 70% of rainfall variability in this region is the result of mesoscale convective systems (MCSs; Nesbitt *et al.*, 2006) initiated in the lee of the high terrain of the Great Rift Valley (GRV; Jackson *et al.*, 2009). The rainfall pattern follows a bimodal distribution with peaks in the March–April–May (MAM) and September–October–November (SON) rainy seasons, with higher amounts occurring during the SON season on average (Jackson *et al.*, 2009). Additional variability in rainfall can be attributed to teleconnections, such as El Niño Southern Oscillation, Atlantic Multi-Decadal Oscillation, Madden-Julian Oscillation (Camberlin *et al.*, 2001; Sandjon *et al.*, 2012; Diem *et al.*, 2014; Berhane *et al.*, 2015), sea surface temperatures (Nicholson and Entekhabi, 1987; Balas *et al.*, 2007; Sinclair *et al.*, 2015), surface-atmosphere coupling, and anthropogenic forcing (Semazzi and Song, 2001; Shem, 2006; Paeth and Thamm, 2007). However, the interactions of these forcing

mechanisms and their relative magnitudes are still not well understood.

Several studies have been performed in and around CEA to determine the size distribution, spatial variability, and temporal frequency of MCSs. MCSs over Africa typically last 11.5 hours (Laing and Fritsch, 1993) and are triggered mainly by elevated terrain (Laing *et al.*, 2011). Coherent episodes of convection occur across several days as they propagate westward from the lee of the GRV. It is thought that they are initiated via thermally induced gravity waves, precipitating and causing feedbacks on successive MCSs via changes in latent and sensible heat fluxes (Nguyen and Duvel, 2008; Laing *et al.*, 2011). Different cloud top temperature (CTT) criteria have been used to identify MCSs in past studies (e.g., Maddox, 1980; Evans and Shemo, 1996), where the criteria vary depending on the study. A few studies have addressed MCSs on a global scale (Vant-Hull *et al.*, 2016; Huang *et al.*, 2018). However, these studies apply their respective criteria across all tropical regions, which hinders capture of some of the regional variability. Geerts and Dejene (2005), for example, use climatologies of Tropical Rainfall Measuring Mission (TRMM) radar observations to show that African MCSs are deeper and less stratiform than Amazonian systems. Zipser *et al.* (2006) also note the enhanced nature of updrafts associated with convection over CEA relative to other regions of the tropics. Other studies address African systems for shorter time periods (e.g., Laing and Fritsch, 1993; Jackson *et al.*, 2009) or for other regions and different time periods (e.g., Taylor *et al.*, 2017).

For these reasons, the present study creates a new 33-year MCS climatology for the MAM and SON rainy seasons for the period 1983–2015 to gain better knowledge of these systems and how they might affect rainfall variability in CEA. Results from the methodology will be compared to prior research in the region. Results from significance testing will be briefly discussed to determine if MCS characteristics and environmental conditions have any statistically significant differences between the two seasons.

## 2 | DATA AND METHODS

To identify and track MCSs, the National Oceanic and Atmospheric Administration (NOAA) National Climatic Data Center (NCDC) 3-hourly gridded satellite data (GridSat-B1) was utilized. GridSat-B1 is on a 0.07° equal-angle grid. The 11  $\mu\text{m}$  infrared window from the Climate Data Record (IRWIN\_CDR) was used to locate minimum CTTs within organized convection. Satellite data have



inherent errors associated with view angle and instrument calibration. Errors from view angle are typically small in the tropics and not considered a factor here. Additionally, GridSat-B1 is an off-shoot of the International Satellite Cloud Climatology Project (ISCCP) calibration, which has been tested and validated (<https://www.ncdc.noaa.gov/cdr/fundamental/geostationary-ir-channel-brightness-temperature-gridsat-b1>). Data gaps and time gaps between seasons are other potential sources of error. However, any effects from these gaps are considered negligible here given the length of the data set and the fact that there might be several hundred MCSs within the domain in any given season.

The National Aeronautics and Space Administration's (NASA) Modern-Era Retrospective analysis for Research and Applications, Version 2 (MERRA2) was also used to create portions of this dataset as they relate to MCS-relative environmental parameters. MERRA2 has a horizontal resolution of  $0.5^\circ$  latitude by  $0.625^\circ$  longitude, contains 42 pressure levels, and has a temporal resolution of 6 hr. This reanalysis was chosen due to its low biases and root mean square error in describing wind fields over CEA. In addition, it has been shown to capture the major features of the seasonal cycle and evolution of rainfall relative to observations (Hua *et al.*, 2019).

## 2.1 | MCS criteria

The definition of a mesoscale convective complex, a type of MCS, was originally developed by Maddox (1980). Successive studies have used similar criteria for identifying, classifying, and tracking MCSs, but to varying degrees over several time periods (e.g., Laing and Fritsch, 1993; Evans and Shemo, 1996; Hodges and Thorncroft, 1997; Laurent *et al.*, 1998). In the present study, MCSs are identified as convective clusters having a  $-48^\circ\text{C}$  CTT contour area. After careful visual inspection of the data, the  $-48^\circ\text{C}$  contour was determined to better represent areas of independent, organized convection over CEA. Warmer CTT thresholds tended to combine systems that were independent through inspection of several convective scenarios. The enhanced nature of updrafts associated with convection over CEA (Zipser *et al.*, 2006) further supported this decision. A  $10,000\text{ km}^2$  CTT contour area threshold was chosen because storms with a length scale smaller than 100 km tend to be more isolated and disorganized. An upper length scale threshold of 1,000 km was also chosen because systems, or collections of systems, that reach this size are considered synoptic scale features. They are not of interest in

the present study due to their potential effects on large-scale circulation patterns and subsequent feedbacks on MCS propagation. In addition to the temperature and size thresholds, their lifecycles must be at least 6 hr long (i.e., three time steps), consistent with prior studies (e.g., Maddox, 1980; Laurent *et al.*, 1998).

## 2.2 | Locating minimum CTTs

The first step towards identifying MCSs was to identify CTT minima within the domain. To locate minima in the GridSat-B1 data, a modified detection algorithm written in the Grid Analysis and Display System (GrADS) was utilized. The original algorithm comes from McKenzie (2017), who used it to identify minimum sea level pressure in tropical cyclones.

GridSat-B1 data was smoothed to eliminate the potential for identification of small-scale, isolated convection. This was done by interpolating IRWIN\_CDR to  $0.5^\circ$  resolution. The method for finding CTT minima consisted of shifting a  $6^\circ \times 6^\circ$  box throughout the domain and locating new coordinates for minima after each shift (Figure 2a). Each shift overlapped the previous by  $3^\circ$  to ensure no minima fell on the edges of the box. Any duplicate CTT minima coordinates were then removed from the data. This was done for each 3-hourly time step for the MAM and SON rainy seasons spanning the 33-year period. Note that box size generally determines the size of convective clusters that are captured (Hart, 2003). Figure 2b provides an example of CTT minima search results from 00Z October 1, 2000.

## 2.3 | Filtering CTT minima

Although smoothing of minimum CTT locations to  $0.5^\circ$  resolution was able to eliminate some small-scale convection, additional filtering was required to eliminate any remaining noise and ensure CTT minima were associated with potential MCSs. Note the term “potential” will be used going forward until the 6-hr duration criterion is applied in the final step of the identification process (Section 2.5).  $0.5^\circ$  coordinates for CTT minima identified in the previous section were introduced into the  $0.07^\circ$  IRWIN\_CDR in order to accurately calculate areas within the  $-48^\circ\text{C}$  CTT contour. It should also be noted that using smoothed coordinates, in many cases, better centred CTT minima within regions of organized convection. However, this was not the case for all minima.

First, to eliminate remaining small-scale convective features, concentric circles were drawn around each coordinate to calculate  $-48^\circ\text{C}$  contour areas at each time step,

## Depictions from the MCS Identification Process

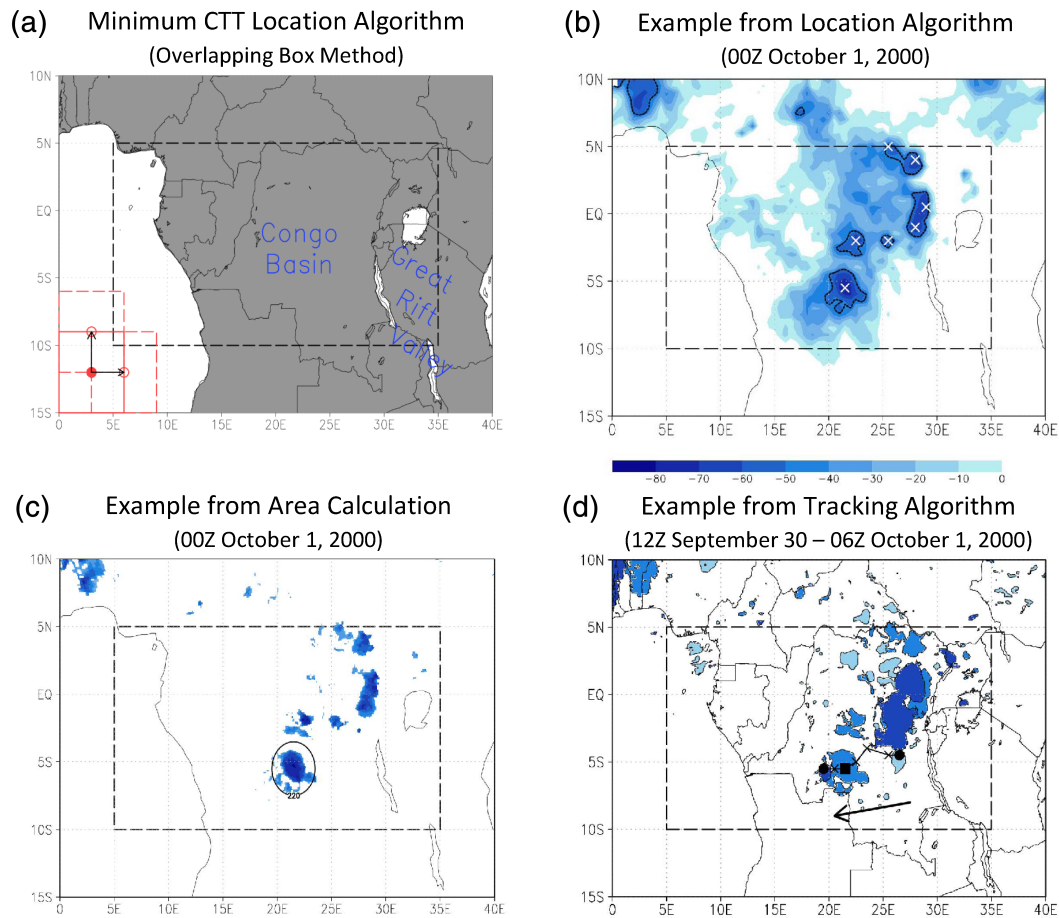


**FIGURE 2** Depictions from the mesoscale convective system (MCS) identification process, with examples provided from an MCS that occurred September 30 to October 1, 2000. (a) The algorithm used to locate CTT minima in IRWIN\_CDR, where smaller boxes with arrows represent the shifting box. (b) Results from (a) for 00Z October 1, 2000, where Xs represent locations of CTT minima and black dashed contours represent the  $-48^{\circ}\text{C}$  contour. (c) The area calculation for 00Z October 1, 2000, where areas are based on pixel counts within  $-48^{\circ}\text{C}$  contours (shaded areas) in the  $0.07^{\circ}$  IRWIN\_CDR and the circle represents the radius of the system (km) using great circle distance. (d) The lifecycle of the MCS, where lighter shades represent  $\leq -48^{\circ}\text{C}$  cloud coverage for 12Z-9/30, medium shades coverage for 00Z-10/1, darker shades coverage for 06Z-10/1, the square marker representing MCS location in (b) and (c), and the arrow indicating direction of propagation. Dashed black boxes represent the domain boundary in all figures [Colour figure can be viewed at [wileyonlinelibrary.com](http://wileyonlinelibrary.com)]

similar to McKenzie (2017) who used this technique to calculate sizes of tropical cyclones. This was done using the great circle distance formula to expand circles around each CTT minimum, and calculating  $-48^{\circ}\text{C}$  contour areas (from the  $0.07^{\circ}$  IRWIN\_CDR) within each expansion of the circle. First, a circle with a 40 km radius (length scale of 80 km) was drawn around each CTT minimum and the area within the  $-48^{\circ}\text{C}$  contour was calculated inside the circle. Note that the length scale of the circle is slightly smaller than the 100 km lower length scale criterion (Section 2.1). Next, a second circle with a radius of 60 km was drawn and the same area calculation was performed. If the  $-48^{\circ}\text{C}$  contour area within the larger circle increased by less than 2% when compared to the

smaller circle, the CTT minimum was excluded. If the percentage increase was greater than or equal to 2% from the first to second circle, the CTT minimum was deemed to be associated with a potential MCS. Starting at a lower length scale effectively isolated and eliminated most remaining small-scale features.

Once small-scale convection was filtered out, the MCS size criteria were applied. As previously stated, a potential MCS must have a  $-48^{\circ}\text{C}$  CTT contour area of at least  $10,000\text{ km}^2$  (Section 2.1). In addition, for purposes related to the area calculation, it must also lie within a circle of radius 80 km (i.e., the area within the  $-48^{\circ}\text{C}$  contour must fill roughly half the circle). Note that a 60 km radius circle has an area of about  $11,300\text{ km}^2$ , very

close to the 10,000 km<sup>2</sup> threshold needed to be of proper size. However, after trial and error analyzing time steps with large convective size distributions, it was decided that 60 km radius circles were not capturing all systems meeting the minimum size requirement. This was caused by several minimum coordinates falling near the edges of organized convection and the −48°C contour area not covering an adequate amount of the circle area. As such, it was found that 80 km radius circles with at least 10,000 km<sup>2</sup> of area coverage represented by the −48°C contour area adequately captured systems of suitable size. If this criterion was met, the algorithm continued expanding circles around CTT minima and calculating the −48°C contour area within each circle (Figure 2c). If the −48°C contour area within a circle increased by less than 2% from its predecessor, the system was deemed a potential MCS and the area calculation from the preceding time step would represent the size of the convective area. Additionally, if the percentage growth of the −48°C contour area within a circle exceeded that of its predecessor, the system was also deemed a potential MCS. This created less likelihood for inclusion of adjacent systems that would produce a high bias for maximum area/size calculations. If the radius reached 500 km (i.e., a length scale of 1,000 km – Section 2.1), the system was no longer deemed a mesoscale feature and was eliminated. Such a system would have the potential to affect circulation patterns (e.g., due to large-scale latent heat release) and is beyond the scope of this study.

## 2.4 | Connecting CTT minima through time

To track potential MCSs through time, a tracking algorithm developed by Hart (2003) was modified to track CTT minima instead of minimum sea level pressure. The algorithm was given radii for where and how far to search while connecting coordinates through time. Search radii are preferred here over the area-overlapping method, since the area-overlapping method is less likely to capture fast-moving MCSs, like squall lines, and assumes that the location and area of MCSs do not change significantly throughout their lifecycles (Huang *et al.*, 2018). Capturing fast-moving MCSs can be a weakness using search radii as well. However, to combat this potential weakness here, a 250-km westward search radius was chosen, since MCSs over CEA have been well documented to propagate westward. Since little eastward propagation of MCSs has been observed in the past, a 125-km eastward search constraint was applied to account for any slight eastward propagation that might occur. The oval-like search areas created by the search

radii also account for northward and southward propagation.

The algorithm starts at the first time step in the data set and creates track files for the initial and succeeding time steps. Coordinates in the initial time step are matched to coordinates in the successive time step using the search radii. Coordinates from both time steps that are closest in distance and within the search constraints are determined to be of the same system. If coordinates in the initial track file are not matched to any successive coordinates, then the system is deemed to expire. Conversely, coordinates that are not matched in the succeeding track file are considered potential initiation locations for new MCSs. The algorithm then shifts forward in time and the process repeats. An example of this process is shown in Figure 2d. The algorithm continues to loop through the dataset in this fashion while recording the following for each time step:

- 1 Number of the MCS that was initiated (chronological)
- 2 Time step number (MCS-relative)
- 3 Date and time (YYYYMMDDHH)
- 4 Latitude/longitude coordinate (decimal degrees)
- 5 Minimum CTT (°C)
- 6 MCS radius (km)
- 7 −48°C CTT contour area (km<sup>2</sup>)
- 8 Percentage change in the −48°C CTT contour area from the preceding time step
- 9 Percentage of circle covered by the −48°C CTT contour area

## 2.5 | Applying the duration criterion and calculating parameters

The data set was filtered to eliminate potential MCSs whose lifecycles were less than 6 hours. In the tropics, it is important to consider shear below mid-level jets, such as the AEJ-N (Zipser *et al.*, 2006) and its southern counterpart, the AEJ-S (Jackson *et al.*, 2009). Low-level equivalent potential temperature ( $\theta_e$ ) is also an important consideration, as it serves as a measure of instability in the lower troposphere and can be used to indicate heat and moisture transport (Hanft and Houston, 2018). As such, environmental parameters were calculated using MERRA2 at and below 650 hPa, since both AEJ cores favor this level. The following propagation and environmental parameters were calculated for all MCSs:

- 1 MCS total displacement (km) – using great circle distance
- 2 MCS duration (hours)
- 3 MCS speed (m s<sup>−1</sup>)

- 4 MCS trajectory ( $^{\circ}$ ) – direction towards which propagation occurred, but using meteorological degrees (i.e., north =  $0/360^{\circ}$ , east =  $90^{\circ}$ , south =  $180^{\circ}$ , and west =  $270^{\circ}$ )
- 5 Extreme and average minimum CTTs ( $^{\circ}\text{C}$ )
- 6 Maximum and average  $-48^{\circ}\text{C}$  contour areas ( $\text{km}^2$ )
- 7 Average 650 hPa wind speed ( $\text{m s}^{-1}$ ) and direction ( $^{\circ}$ ) – refer to Parameter 4 above for direction
- 8 Average surface-650 hPa vertical shear magnitude ( $\text{m s}^{-1}$ ) and direction ( $^{\circ}$ ) – refer to Parameter 4 above for direction
- 9 Average 650 hPa relative vorticity ( $\text{s}^{-1}$ )
- 10 Average surface-650 hPa  $\theta_e(\text{K})$

## 2.6 | Regional comparisons and differences between seasons

Once all parameters were obtained, MCSs were separated by region based on where they were initiated. Region 1 spans from  $1^{\circ}$ – $5^{\circ}\text{N}$ , Region 2 from  $0^{\circ}$ – $5^{\circ}\text{S}$ , and Region 3 from  $6^{\circ}$ – $10^{\circ}\text{S}$  (Figure 1). The division of the domain into regions was due to meridional variations in vertical shear, terrain, and proximity to the Equator. The general east-to-west propagation of MCSs also supports this division because MCSs are less likely to propagate outside their respective regions of origin than if regions were divided by longitude. This allows for better assessment of factors influencing their behaviour on a regional basis. Time series of MCS and environmental parameter means for the domain and individual regions were plotted. Best-fit lines and  $r^2$  values were also calculated to indicate if any variability could be explained in the dataset.

Several parameters had skewed distributions for both seasons. As such, bootstrapping was applied to all parameters, except MCS counts. The number of random samples for each season was based on that season's total 33-year MCS count. Random samples were then averaged and the process was repeated for  $10^4$  iterations. This provided normally distributed populations of sample means with the distribution mean hovering around the true mean, thereby satisfying the Central Limit Theorem. 99% confidence intervals (CIs) were calculated for a given parameter for both seasons to determine if they overlapped. If CIs overlapped, then there was no guarantee that differences between randomly sampled MCSs from each season, for a given parameter, would be statistically significant. If CIs did not overlap, then it could be deduced that MCSs, for a given parameter, would be significantly different at that CI. Note that the rejection/acceptance of the null hypothesis does not allude to why differences between the seasons exist/do not exist,

respectively. It is simply a conditional statement. Explanations for differences will need to be addressed through analysis.

Distributions of MCS counts approached Gaussian for both seasons (not shown). Since there are 33 years of data, a z-test was performed to determine whether differences between MAM and SON MCS counts were statistically significant. Differences between seasons were statistically significant if the z-score reached the 99% confidence level.

## 3 | RESULTS

### 3.1 | Spatial patterns

Figure 3 depicts maps representing spatial distributions of MCS parameter means based on their initiation locations. There are consistent patterns in MCS activity between MAM and SON (Figure 3a): the hot spot over Lake Victoria (near  $1^{\circ}\text{S}$ ,  $33^{\circ}\text{E}$ ), hot spots west of the Rwenzori and Mitumba Ranges ( $0^{\circ}$ – $4^{\circ}\text{S}$ ,  $28^{\circ}\text{E}$ ) and the Blue Mountains ( $2^{\circ}\text{N}$ ,  $29^{\circ}\text{E}$ ), and the hot spot near coastal Cameroon (near  $4^{\circ}\text{N}$ ,  $8^{\circ}\text{E}$ ). The hot spot over Lake Victoria is a nocturnal maximum associated with convergence of mountain/valley breeze circulations over the lake provoking intense thunderstorms (Yin and Nicholson, 1998). The hot spots in the lee of the GRV and Mount Cameroon are the result of prevailing easterly flow (Figure 4a), leading to thermally induced gravity waves (Jackson *et al.*, 2009). Another interesting feature is shown in the 650 hPa vorticity pattern from MERRA2 (Figure 4b). A vorticity couplet appears near  $3^{\circ}\text{S}$ ,  $28^{\circ}\text{E}$ , corresponding to the hot spot in the lee of the Rwenzori and Mitumba ranges in western portions of the Democratic Republic of the Congo. This vorticity couplet also appears in the National Centers for Environmental Prediction's Climate Forecast System Reanalysis (not shown). The author has seen no mention of this feature in the literature. This has potential implications for further research into the effects of mesoscale features on rainfall variability in the Congo basin. Other hot spots along the Atlantic coast can be seen to have seasonal dependency and strongly correspond spatially to regions with elevated terrain during MAM (Figure 1). This supports results from Laing *et al.* (2011), who showed that MCSs are also initiated via land/sea breezes and elevated terrain over tropical Africa. In addition, the cold Benguela current flowing northward along the West African coastline can produce a more pronounced land-sea temperature contrast. This may further aid MCS initiation through localized enhancements of the sea breeze circulation (Jury, 2010; Howard and



## Spatial Distributions of 33-year MCS Counts and Parameter Means based on Initiation Location (1983-2015)

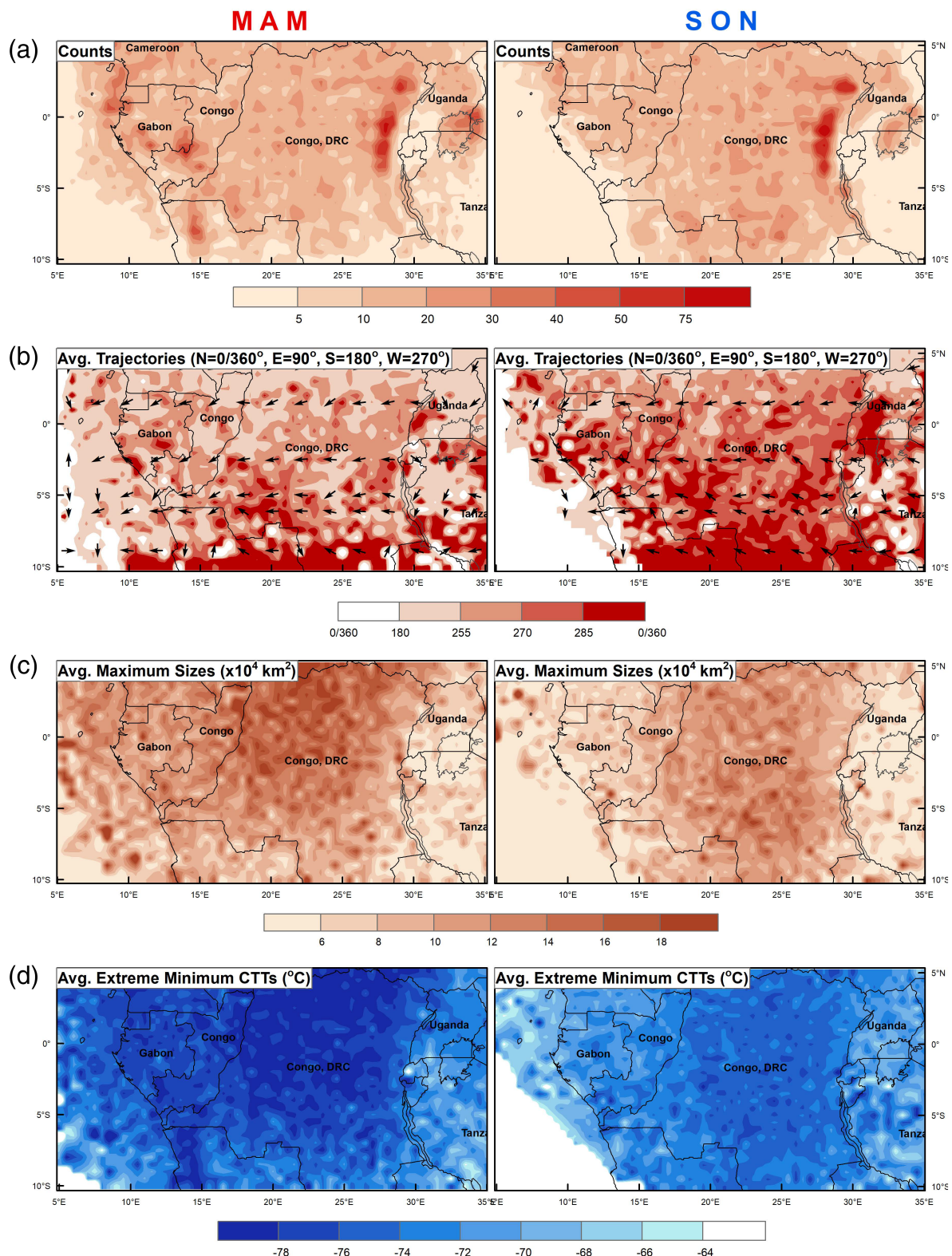


**FIGURE 3** 33-year (1983–2015) mesoscale convective system (MCS) counts and parameter means based on initiation locations at  $0.5^{\circ}$  resolution: (a) MCS counts, (b) trajectories ( $^{\circ}$ ), where arrows represent nearest-neighbor interpolated trajectories at  $2^{\circ}$  resolution, (c) extreme maximum areas ( $\text{km}^2$ ), (d) extreme minimum cloud top temperatures ( $^{\circ}\text{C}$ ), (e) speeds ( $\text{m s}^{-1}$ ), (f) durations (hours), and (g) displacements (km) [Colour figure can be viewed at [wileyonlinelibrary.com](http://wileyonlinelibrary.com)]

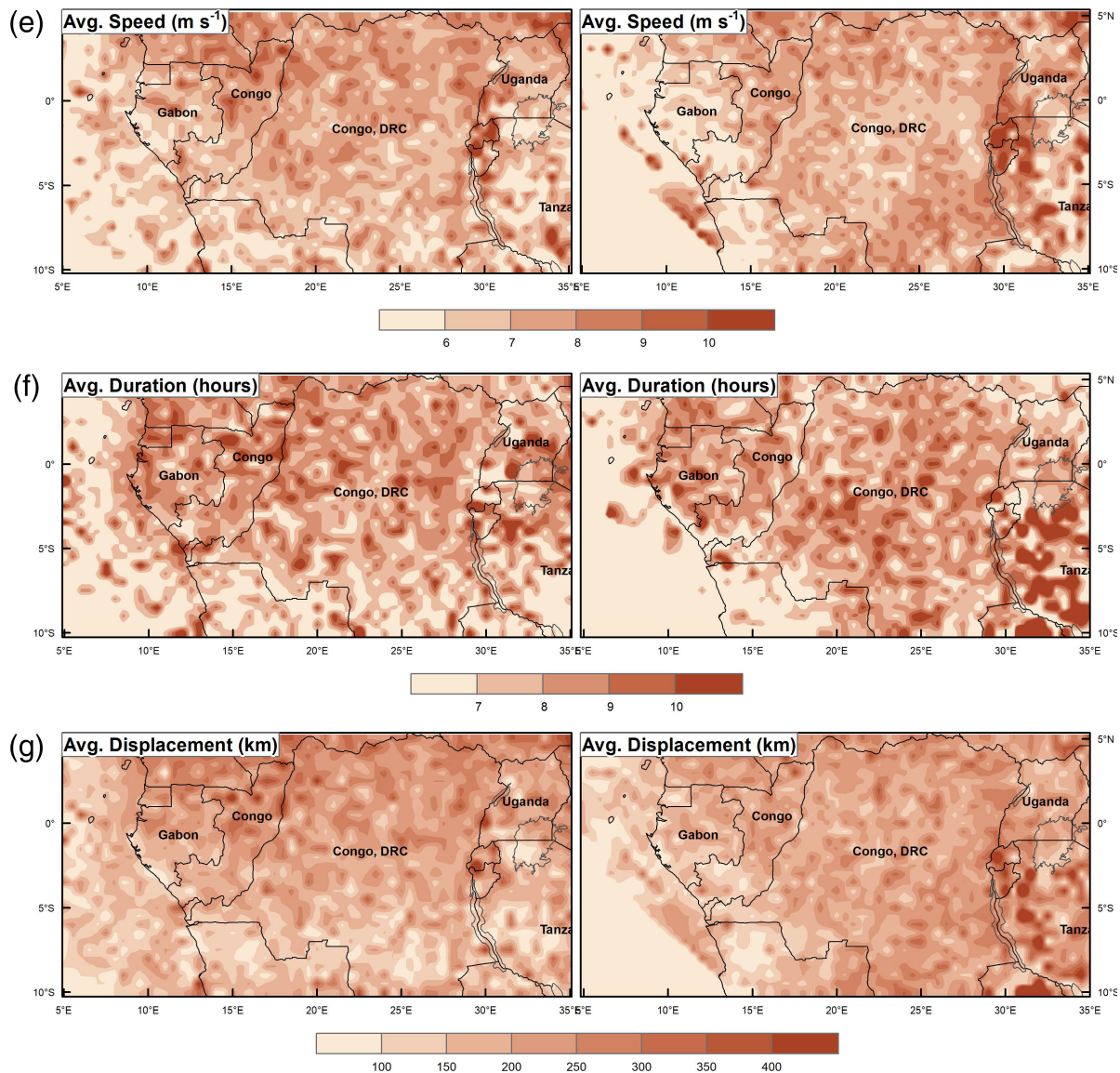


**FIGURE 3** (Continued)

Washington, 2018). Balas *et al.* (2007) also suggested a strong link and seasonal dependency between Atlantic SSTs and West African rainfall variability. During the SON rainy season, there is a stark reduction in the number of active areas along the coastline. Jackson *et al.* (2009) suggest that the annual oscillation of maximum insolation may be an important factor in the spatial distribution of MCSs over CEA.

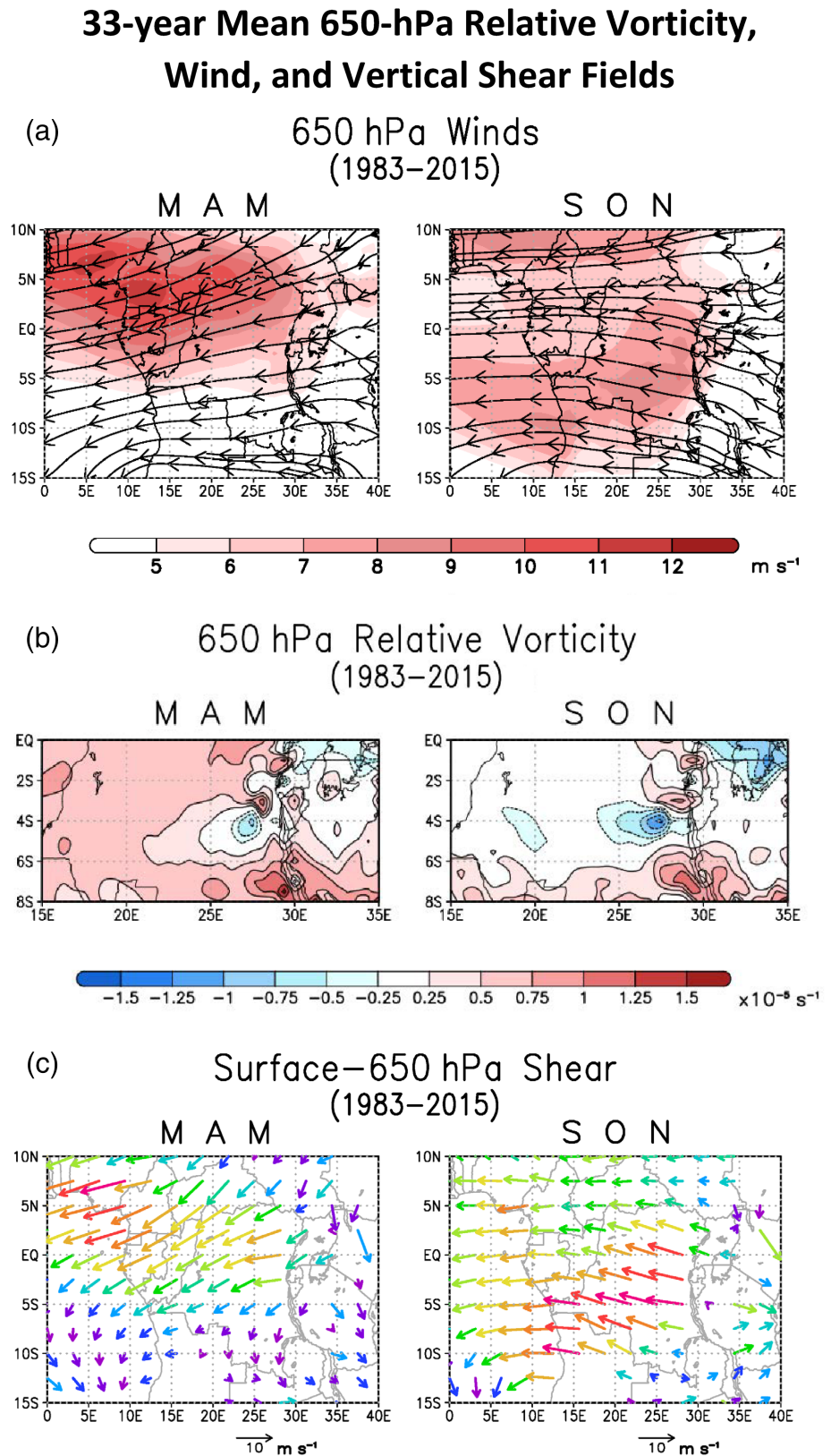
MCS trajectories are generally westward throughout the domain (Figure 3b), consistent with prior studies (Laing and Fritsch, 1993; Hodges and Thorncroft, 1997; Laing *et al.*, 2008; 2011). MAM MCSs tend to have a larger westward component to their propagation in Regions 2 and 3, compared to SON. Region 1 exhibits greater consistency in overall track, with some increased variation

near the Equator. However, major factors that are steering these systems cannot be discerned directly from this study.

Figure 3c,d shows the average maximum sizes and intensities, respectively, reached by MCSs based on where they initiate. There are clear differences between land and ocean MCSs. MCSs in MAM grow to reach greater than 120,000 km<sup>2</sup> across large portions of Region 1 and Region 2, contrary to the SON season, where larger MCSs tend to favor only the Congo basin. Notice that the Congo basin is a favorable location for systems to grow larger than in surrounding areas in both seasons. This may be indicative of moisture recycling via evapotranspiration (Pokam *et al.*, 2012; Dyer *et al.*, 2017) or via preceding MCSs precipitating and causing feedbacks on successive systems (Nguyen



**FIGURE 4** 33-year (1983–2015) mean 650 hPa meteorological fields from MERRA2 for March–April–May (MAM) and September–October–November (SON): (a) winds ( $\text{m s}^{-1}$ ) and streamlines, (b) relative vorticity ( $\text{s}^{-1}$ ), where dotted/solid contours indicate negative/positive vorticity, and (c) Surface–650 hPa shear vectors ( $\text{m s}^{-1}$ ) [Colour figure can be viewed at [wileyonlinelibrary.com](http://wileyonlinelibrary.com)]



and Duvel, 2008; Laing *et al.*, 2011). However, further analysis is needed to determine the effects of low-level moisture on MCS size here. The spatial distribution of maximum intensities is very similar to that for

maximum sizes achieved (Figure 3d) and show that MCSs reach greater intensities over land than ocean, consistent with prior research (Futyan and Del Genio, 2007; Huang *et al.*, 2018).

### Diurnal Cycles for MCS Counts, Maximum Size, and Maximum Intensity Averaged Over the Domain

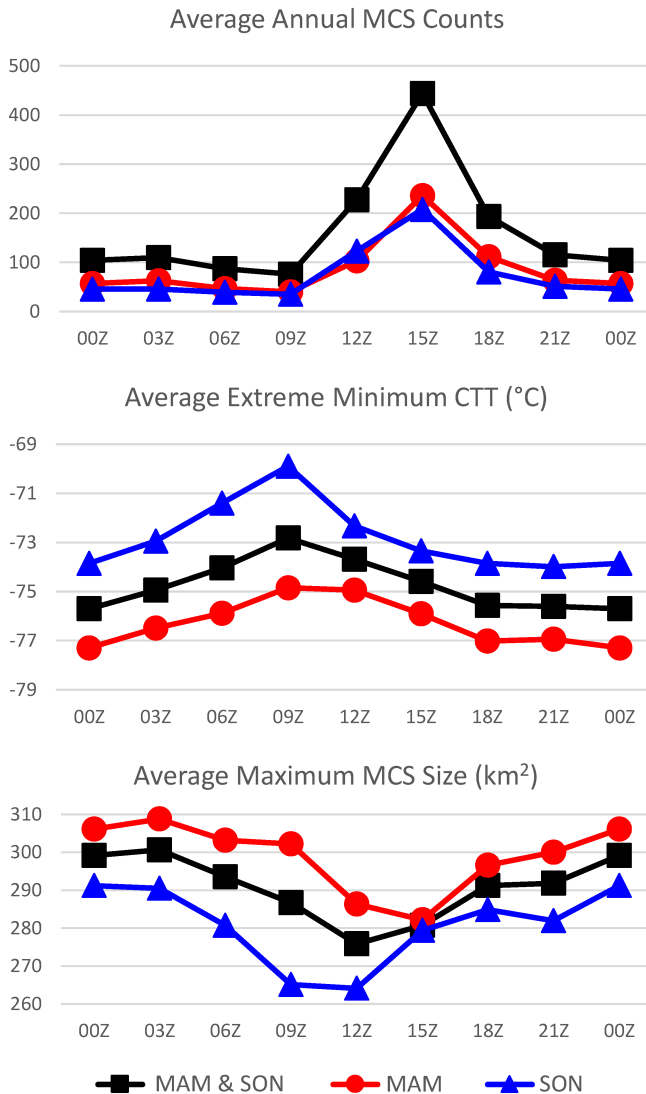


**FIGURE 5** Diurnal cycles for average annual mesoscale convective system counts, extreme minimum cloud top temperatures (°C) (i.e., maximum intensity), and maximum sizes achieved (km<sup>2</sup>) [Colour figure can be viewed at [wileyonlinelibrary.com](http://wileyonlinelibrary.com)]

MCSs are also shown propagate more than  $9 \text{ m s}^{-1}$  over several land areas, particularly Region 1, but drop off to  $7\text{--}9 \text{ m s}^{-1}$  near and over the Atlantic (Figure 3e), similar to results from Hodges and Thorncroft (1997), who used ISCCP Meteosat imagery to determine the distribution and characteristics of African MCSs. In addition, MCSs last more than 8 hours over much of the Congo basin, with several locations averaging over 9 and 10 hours (Figure 3f), consistent with Huang *et al.* (2018) and Laing and Fritsch (1993). Patterns for

MCS duration and displacement (Figure 3f,g, respectively) correspond well spatially in both MAM and SON with the 650 hPa average wind and low-level vertical shear fields (Figure 4a,c, respectively). The feature that develops in Figure 4a,c along the southern rim of the Congo basin extending towards the Atlantic during SON is known as the southern branch of the AEJ (AEJ-S). This feature is thought to be the result of the large meridional temperature gradient between the Angola heat low and the persistent convection over the Congo basin (Adebiyi and Zuidema, 2016). The present study can only speculate about the relationship between low-level shear and evolution and sustainability of MCSs. However, several studies (e.g., Zipser *et al.*, 2006; Jackson *et al.*, 2009) argue the importance of considering shear below mid-level jets, such as the AEJ-N and AEJ-S, as it pertains to intensity and evolution of MCSs. Laing *et al.* (2011) also show the importance of moderate low-level vertical shear as it pertains to the evolution of MCSs initiated in the proximity of high terrain. As such, these potential relationships will require further investigation and offer an avenue for future research.

### 3.2 | Diurnal cycle

The diurnal cycle for convective episodes (Figure 5) agrees well with the literature. On average over the domain, MCS initiation frequency is greatest in the afternoon near 15Z, consistent with Jackson *et al.* (2009), who found similar results using the TRMM database from the University of Utah, and Huang *et al.* (2018). MCSs are least likely to initiate near 09Z, as Jackson *et al.* (2009) also showed. MCSs tend to reach their maximum intensities during the nighttime hours. Times when MCSs reach their maximum intensities match up well with when they reach their maximum sizes. However, the correlation between these parameters is small among individual systems. In other words, for any given MCS, maximum size and intensity will not always occur at the same time during its lifecycle.

### 3.3 | Differences between rainy seasons

Table 1 shows MAM and SON normalized parameter means whose differences are statistically significant at the 99% CI. One main pattern to recognize is the great consistency with which MCSs propagate through the domain with regard to displacement, duration and speed. Much of this consistency can be attributed to Region 2. Differences between MAM and SON environmental



**TABLE 1** Statistical significance of differences between March–April–May(MAM) and September–October–November(SON) mesoscale convective system propagation and environmental parameters for the domain and individual regions. Xs indicate statistical significance at the 99% confidence interval.

| Parameter   |                    | Domain | R1 | R2 | R3 |
|-------------|--------------------|--------|----|----|----|
| Propagation | Number of events   | ×      | ×  | ×  |    |
|             | Displacement       |        | ×  |    | ×  |
|             | Duration           |        | ×  |    | ×  |
|             | Speed              |        | ×  |    | ×  |
|             | Trajectory         | ×      |    | ×  | ×  |
| Environment | Ext. min. CTT      | ×      | ×  | ×  | ×  |
|             | Ext. max. area     | ×      | ×  | ×  | ×  |
|             | Wind speed         | ×      | ×  | ×  | ×  |
|             | Wind direction     | ×      | ×  | ×  | ×  |
|             | Shear              | ×      | ×  |    | ×  |
|             | Shear direction    | ×      | ×  | ×  | ×  |
|             | Relative vorticity | ×      | ×  | ×  |    |
|             | Equiv. pot. temp   | ×      | ×  | ×  | ×  |

Abbreviations: CTT, cloud top temperature.

### 33-year Time Series of Extreme Minimum CTTs and Low-level Equivalent Potential Temperatures Averaged over the Domain

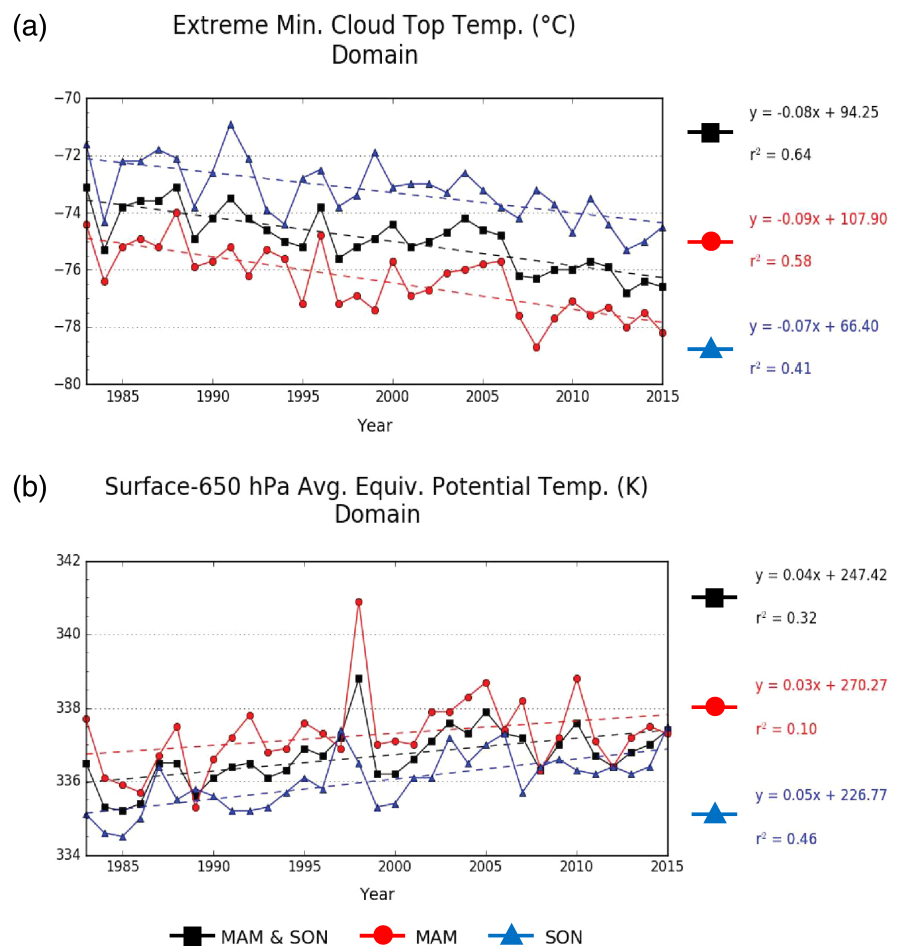


**FIGURE 6** 33-year (1983–2015) time series of annual extreme minimum cloud top temperatures (a; °C) averaged and low-level  $\theta_e$  (b; K) averaged over the domain [Colour figure can be viewed at [wileyonlinelibrary.com](http://wileyonlinelibrary.com)]

### Zonal Cross-section of $\theta_e$ Averaged over the Domain (1983–2015)

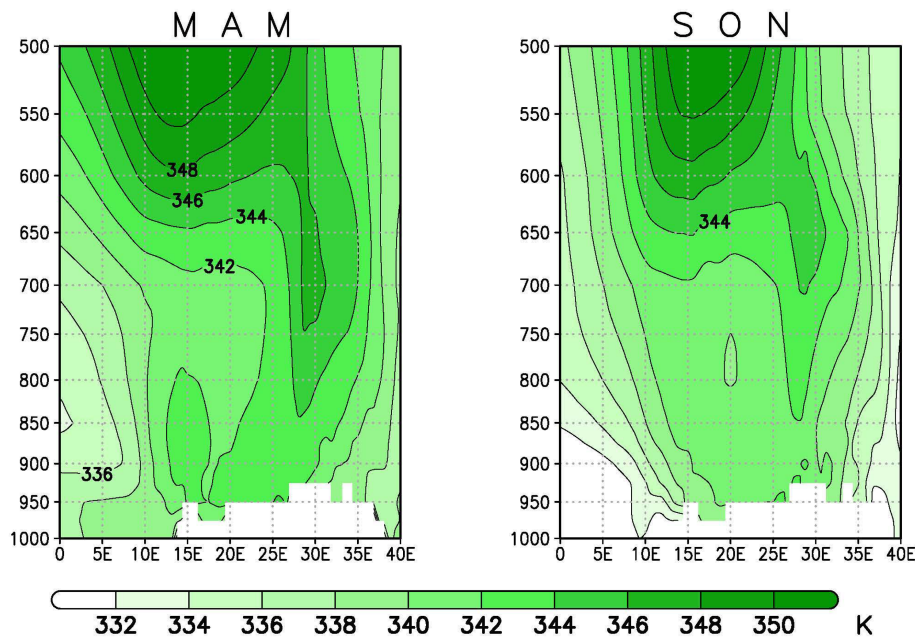


**FIGURE 7** Zonal cross-section of  $\theta_e$ (K) for March–April–May(MAM) and September–October–November(SON) averaged over the domain and over the 33-year period (1983–2015) [Colour figure can be viewed at [wileyonlinelibrary.com](http://wileyonlinelibrary.com)]

parameter means were found to be significantly different in most cases.

Little can be discerned from the interannual variability in the data over the 33-year period. Only low-level  $\theta_e$  and extreme minimum CTTs had variability that could be explained in some capacity by a linear model. 58% and 41% of variability in maximum intensity could be explained by linear models for the MAM and SON seasons (Figure 6a). 46% of variability in low-level  $\theta_e$  could be explained by the linear model for SON (Figure 6b). Overall, MAM tends to have greater low-level  $\theta_e$  and intensities (i.e., lower minimum CTTs achieved) than SON over the entire domain. In addition, MAM exhibits a greater vertical gradient in  $\theta_e$  on average over the domain between the surface and 650 hPa than SON, where  $\theta_e$  is more homogeneous in the lower troposphere (Figure 7). Higher  $\theta_e$  also occurs over elevated terrain near coastal areas during MAM, which corresponds with increased MCS activity along western portions of the Congo basin, near northern Angola, Congo, and Gabon (Figure 3a). This high- $\theta_e$  area could be indicative of elevated terrain heating and/or sea breeze circulations resulting in moisture convergence during MAM, but further analysis is needed to verify. However, MCS development via elevated terrain heating and land/sea breeze circulations have been shown to be common mechanisms for MCS development in Africa (Laing *et al.*, 2011; Howard and Washington, 2018). Farther east over the Congo basin,

moisture transport from the Atlantic is generally higher during SON than MAM annually (Dyer *et al.*, 2017). Therefore, higher  $\theta_e$  values during MAM are likely due to evapotranspiration and water recycling (Dyer *et al.*, 2017), as moisture advection is reduced during MAM. Residual heating may also contribute to higher  $\theta_e$  during MAM as maximum insolation shifts northward (Jackson *et al.*, 2009).

## 4 | CONCLUSION

The new 33-year MCS climatology presented here for the MAM and SON rainy seasons agrees well with prior research. The spatial distribution of hot spots of MCS activity further validates prior literature. Hot spots of activity include Lake Victoria, the lee of the GRV and Blue Mountains, and Mount Cameroon. The hot spot in the lee of the GRV (0°–4°S, 28°E) lies in close proximity to a 650 hPa vorticity couplet in MERRA2, and may provide an opportunity for further research into the increased initiation frequency at that location and how it relates to rainfall variability in the Congo basin. Seasonal differences in spatial distributions of MCS activity are also represented well; for example, in the case of the hot spots near and along the Atlantic coast during MAM, where enhanced temperature gradients have been known to lead to sea breeze circulations (Laing *et al.*, 2011). Spatial distributions of maximum sizes and intensities

provide another avenue for future research into the effects of moisture transport and moisture recycling on MCSs (Pokam *et al.*, 2012; Dyer *et al.*, 2017). Average speeds of MCSs also agree well with prior research with regard to MCS propagation over land versus water (Hodges and Thorncroft, 1997).

Diurnal variations in annual MCS counts, maximum intensities, and maximum sizes are in good agreement with prior studies (Jackson *et al.*, 2009; Huang *et al.*, 2018). A distinct peak in initiation frequency exists at 15Z across the domain, coinciding with afternoon heating. Maximum intensities and sizes are generally shown to follow several hours later, on average.

The inclusion of MERRA2 into the dataset provides more accurate representations of environments in which MCSs propagate and thrive. This provides a good basis for future research into rainfall variability over CEA, as MERRA2 has been shown to reproduce spatial variations and interannual variability in rainfall well in this region, in addition to providing low biases in the wind fields (Hua *et al.*, 2019).


Differences between MAM and SON rainy seasons were shown to be statistically significant for most parameters. However, Region 2 centered over the Congo basin shows the greatest consistency between seasons in average MCS displacement, duration, and speed. All parameters exhibited large interannual variability.

The new MCS climatology presented here offers several paths forward for future research in CEA and is available, upon request to the author. It provides a platform, in addition to existing datasets, on which to build and improve upon our understanding of rainfall variability in tropical Africa and its effects on human health and the economies of the region.

## ACKNOWLEDGEMENTS

This work was supported by the National Science Foundation Division of Atmospheric and Geospace Sciences (NSF AGS 1535439 and GEO/ATM 1854511). I would like to thank Dr. Sharon Nicholson for the opportunity and guidance she has provided. Special thanks also goes to Dr. Robert Hart for his extensive assistance with the tracking algorithm necessary for the completion of this research.

## ORCID

Adam T. Hartman  <https://orcid.org/0000-0001-9317-4891>

## REFERENCES

Adebiyi, A. and Zuidema, P. (2016) The role of the southern African easterly jet in modifying the Southeast Atlantic aerosol

and cloud environments. *Quarterly Journal of the Royal Meteorological Society*, 142, 1574–1589. <https://doi.org/10.1002/qj.2765>.

Balas, N., Nicholson, S.E. and Klotter, D. (2007) The relationship of rainfall variability in west Central Africa to sea-surface temperature fluctuations. *International Journal of Climatology*, 27, 1335–1349. <https://doi.org/10.1002/joc.1456>.

Berhane, F., Zaitchik, B. and Badr, H.S. (2015) The Madden-Julian Oscillation's influence on spring rainy season precipitation over equatorial West Africa. *Journal of Climate*, 28, 8653–8672. <https://doi.org/10.1175/JCLI-D-14-00510.1>.

Camberlin, P., Janicot, S. and Pocard, I. (2001) Seasonality and atmospheric dynamics of the teleconnection between African rainfall and tropical sea-surface temperature: Atlantic vs. ENSO. *International Journal of Climatology*, 21, 973–1005. <https://doi.org/10.1002/joc.673>.

Camberlin, P., Barraud, G., Bigot, S., Dewitte, O., Imwangana, F. M., Mateso, J. M., Martiny, N., Monsieus, E., Moron, V., Pellarin, T., Philippon, N., Sahani, M. & Samba, G. (2019) Evaluation of remotely sensed rainfall products over Central Africa. *Quarterly Journal of the Royal Meteorological Society*, 145, 2115–2138. <https://doi.org/10.1002/qj.3547>.

Diem, J.E., Ryan, S.J., Hartter, J. and Palace, M.W. (2014) Satellite-based rainfall data reveal a recent drying trend in central equatorial Africa. *Climatic Change*, 126, 263–272. <https://doi.org/10.1007/s10584-014-1217-x>.

Dyer, E.L.E., Jones, D.B.A., Nusbaumer, J., Li, H., Collins, O., Vettoretti, G. and Noone, D. (2017) Congo Basin precipitation: assessing seasonality, regional interactions, and sources of moisture. *Journal of Geophysical Research – Atmospheres*, 122, 6882–6898. <https://doi.org/10.1002/2016JD026240>.

Evans, J.L. and Shemo, R.E. (1996) A procedure for automated satellite-based identification and climatology of development of various classes of organized convection. *Journal of Applied Meteorology and Climatology*, 35, 638–652. [https://doi.org/10.1175/1520-0450\(1996\)035<0638:APFASB>2.0.CO;2](https://doi.org/10.1175/1520-0450(1996)035<0638:APFASB>2.0.CO;2).

Futyan, J.M. and Del Genio, A. (2007) Deep convective system evolution over Africa and the tropical Atlantic. *Journal of Climate*, 20, 5041–5060. <https://doi.org/10.1175/JCLI4297.1>.

Geerts, B. and Dejene, T. (2005) Regional and diurnal variability of the vertical structure of precipitation systems in Africa based on spaceborne radar data. *Journal of Climate*, 18, 893–916.

Hanft, W. and Houston, A.L. (2018) An observational and modeling study of mesoscale air masses with high theta-e. *Monthly Weather Review*, 146, 2503–2524. <https://doi.org/10.1175/MWR-D-17-0389.1>.

Hart, R.E. (2003) A cyclone phase space derived from thermal wind and thermal asymmetry. *Monthly Weather Review*, 131, 585–616. [https://doi.org/10.1175/1520-0493\(2003\)131<0585:ACPSDF>2.0.CO;2](https://doi.org/10.1175/1520-0493(2003)131<0585:ACPSDF>2.0.CO;2).

Hodges, K.I. and Thorncroft, C.D. (1997) Distribution and characteristics of African mesoscale convective weather systems based on the ISCCP Meteosat imagery. *Monthly Weather Review*, 125, 2821–2837. [https://doi.org/10.1175/1520-0493\(1997\)125<2821:DASOAM>2.0.CO;2](https://doi.org/10.1175/1520-0493(1997)125<2821:DASOAM>2.0.CO;2).

Howard, E. and Washington, R. (2018) Characterizing the synoptic expression of the Angola low. *Journal of Climate*, 31, 7147–7165. <https://doi.org/10.1175/JCLI-D-18-0017.1>.

- Hua, W., Zhou, L., Nicholson, S.E., Chen, H. and Qin, M. (2019) Assessing reanalysis data for understanding rainfall climatology and variability over central equatorial Africa. *Climate Dynamics*, 53, 651–669. <https://doi.org/10.1007/s00382-018-04604-0>.
- Huang, X., Hu, C., Huang, X., Chu, Y., Tseng, Y., Zhang, G.J. and Lin, Y. (2018) A long-term tropical mesoscale convective systems dataset based on a novel objective automatic tracking algorithm. *Climate Dynamics*, 51, 3145–3159. <https://doi.org/10.1007/s00382-018-4071-0>.
- Jackson, B., Nicholson, S.E. and Klotter, D. (2009) Mesoscale convective systems over western equatorial Africa and their relationship to large-scale circulation. *Monthly Weather Review*, 137, 1272–1294. <https://doi.org/10.1175/2008MWR2525.1>.
- Jury, M. (2010) Climate and weather factors modulating river flows in southern Angola. *International Journal of Climatology*, 30, 901–908. <https://doi.org/10.1002/joc.1936>.
- Laing, A.G. and Fritsch, J.M. (1993) Mesoscale convective complexes in Africa. *Monthly Weather Review*, 121, 2254–2263. [https://doi.org/10.1175/1520-0493\(1993\)121<2254:MCCIA>2.0.CO;2](https://doi.org/10.1175/1520-0493(1993)121<2254:MCCIA>2.0.CO;2).
- Laing, A.G., Carbone, R., Levizzani, V. and Tuttle, J. (2008) The propagation and diurnal cycles of deep convection in northern tropical Africa. *Quarterly Journal of the Royal Meteorological Society*, 134, 93–109. <https://doi.org/10.1002/qj.194>.
- Laing, A.G., Carbone, R. and Levizzani, V. (2011) Cycles and propagation of deep convection over equatorial Africa. *Monthly Weather Review*, 139, 2832–2853. <https://doi.org/10.1175/2011MWR3500.1>.
- Laurent, H., D'Amato, N. and Lebel, T. (1998) How important is the contribution of mesoscale convective complexes to the Sahelian rainfall? *Physics and Chemistry of the Earth*, 23, 629–633. [https://doi.org/10.1016/S0079-1946\(98\)00099-8](https://doi.org/10.1016/S0079-1946(98)00099-8).
- Liebmann, B., Bladé, I., Kiladis, G.N., Carvalho, L.M.V., Senay, G. B., Allured, D., Leroux, S. and Funk, C. (2012) Seasonality of African precipitation from 1996 to 2009. *Journal of Climate*, 25, 4304–4322. <https://doi.org/10.1175/JCLI-D-11-00157.1>.
- Maddox, R.A. (1980) Mesoscale convective complexes. *Bulletin of the American Meteorological Society*, 61, 1374–1387.
- McKenzie, T. B. (2017) A climatology of tropical cyclone size in the western North Pacific using an alternative metric. *Master's thesis, Florida State University*, <https://fsu.digital.flvc.org/islandora/object/fsu:507708/datastream/PDF/view>. Accessed 1 Jan. 2019.
- Nesbitt, S.W., Cifelli, R. and Rutledge, S.A. (2006) Storm morphology and rainfall characteristics of TRMM precipitation features. *Monthly Weather Review*, 134, 2702–2721. <https://doi.org/10.1175/MWR3200.1>.
- Nguyen, H. and Duvel, J.P. (2008) Synoptic wave perturbations and convective systems over equatorial Africa. *Journal of Climate*, 21, 6372–6388. <https://doi.org/10.1175/2008JCLI2409.1>.
- Nicholson, S.E. and Entekhabi, D. (1987) Rainfall variability in equatorial and southern Africa: relationships with sea surface temperatures along the southwestern coast of Africa. *Journal of Climate and Applied Meteorology*, 26, 561–578. [https://doi.org/10.1175/1520-0450\(1987\)026<0561:RVIEAS>2.0.CO;2](https://doi.org/10.1175/1520-0450(1987)026<0561:RVIEAS>2.0.CO;2).
- Paeth, H. and Thamm, H.P. (2007) Regional modelling of future African climate north of 15°S including greenhouse warming and land degradation. *Climatic Change*, 83, 401–427. <https://doi.org/10.1007/s10584-006-9235-y>.
- Pokam, W.M., Djiotang, L.A.T. and Mkankam, F.K. (2012) Atmospheric water vapor transport and recycling in equatorial Central Africa through NCEP/NCAR reanalysis data. *Climate Dynamics*, 38, 1715–1729.
- Sandjon, A.T., Nzeukou, A. and Tchawoua, C. (2012) Intraseasonal atmospheric variability and its interannual modulation in Central Africa. *Meteorology and Atmospheric Physics*, 117, 167–179. <https://doi.org/10.1007/s00703-012-0196-6>.
- Semazzi, F.H.M. and Song, Y. (2001) A GCM study of climate change induced by deforestation in Africa. *Climate Research*, 17, 169–182. <https://doi.org/10.3354/cr017169>.
- Shem, W. O. (2006) Biosphere-atmosphere interaction over the Congo basin and its influence on the regional hydrological cycle. *Ph.D. dissertation, Georgia Institute of Technology*, <http://hdl.handle.net/1853/11558>. Accessed 1 Jan. 2019.
- Sinclair, Z., Lenouo, A., Tchawoua, C. and Janicot, S. (2015) Synoptic kelvin type perturbation waves over Congo basin over the period 1979–2010. *Journal of Atmospheric and Solar - Terrestrial Physics*, 130–131, 43–56. <https://doi.org/10.1016/j.jastp.2015.04.015>.
- Taylor, C. M., Belusic, D., Guichard, F., Parker, D. J., Vischel, T., Bock, O., Harris, P. P., Janicot, S., Klein, C. & Panthou, G. (2017) Frequency of extreme Sahelian storms tripled since 1982 in satellite observations. *Nature*, 544 475–478. <https://doi.org/10.1038/nature22069>.
- Vant-Hull, B., Rossow, W. and Pearl, C. (2016) Global comparisons of regional life cycle properties and motion of multiday convective systems: tropical and Midlatitude land and ocean. *American Meteorological Society*, 29, 5837–5858. <https://doi.org/10.1175/JCLI-D-15-0698.1>.
- Washington, R., James, R., Pearce, H., Pokam, W.M. and Moufouma-Okia, W. (2013) Congo Basin rainfall climatology: can we believe the climate models? *Philosophical Transactions of the Royal Society B*, 368, 20120296. <https://doi.org/10.1098/rstb.2012.0296>.
- Yin, X. and Nicholson, S.E. (1998) The water balance of Lake Victoria. *Hydrological Sciences Journal*, 43(5), 789–812. <https://doi.org/10.1080/02626669809492173>.
- Zipser, E.J., Cecil, D.J., Liu, C., Nesbitt, S.W. and Yorty, D.P. (2006) Where are the most intense thunderstorms on earth? *Bulletin of the American Meteorological Society*, 87, 1057–1071. <https://doi.org/10.1175/BAMS-87-8-1057>.

**How to cite this article:** Hartman AT. Tracking mesoscale convective systems in central equatorial Africa. *Int J Climatol*. 2021;41:469–482. <https://doi.org/10.1002/joc.6632>